II

Paper II

8.2 Structure of lateral two-electron quantum dot molecules in electromagnetic fields

V. Popsueva, R. Nepstad, T. Birkeland, M. Førre, J. P. Hansen, E. Lindroth, and E. Waltersson

Physical Review B, **76**, 035303 (2007)

PHYSICAL REVIEW B **76**, 035303 (2007)

Structure of lateral two-electron quantum dot molecules in electromagnetic fields

V. Popsueva,[1] R. Nepstad,[1] T. Birkeland,[2] M. Førre,[1] J. P. Hansen,[1] E. Lindroth,[3] and E. Waltersson[3]
[1]*Department of Physics and Technology, University of Bergen, N-5020 Bergen, Norway*
[2]*Department of Mathematics, University of Bergen, N-5020 Bergen, Norway*
[3]*Atomic Physics, Fysikum, Stockholm University, S-106-91 Stockholm, Sweden*
(Received 10 January 2007; revised manuscript received 19 April 2007; published 3 July 2007)

The energy levels of laterally coupled parabolic double quantum dots are calculated for varying interdot distances. Electron-electron interaction is shown to dominate the spectra: In the diatomic molecule limit of large interdot separation, the two nearly degenerate singlet and triplet ground states are followed by a narrow band of four singlet and four triplet states. The energy spacing between the ground state and the first band of excited states scales directly with the confinement strength of the quantum wells. Similar level separation and band structure are found when the double dot is exposed to a perpendicular magnetic field. Conversely, an electric field parallel to the interdot direction results in a strong level mixing and a narrow transition from a localized state to a covalent diatomic molecular state.

DOI: 10.1103/PhysRevB.76.035303 PACS number(s): 73.21.La, 73.22.−f, 75.75.+a, 85.35.Be

I. INTRODUCTION

Coupled quantum dots typically containing a few "active" electrons have set a new scene for research in molecular physics and have, in many contexts, been named "artificial molecules."[1] Electron tunneling from one well to another typically occurs on nanosecond time scales, which opens for precise manipulation and measurement of electronic states.[2] Two coupled quantum dots containing two electrons thus define a two-dimensional analog to the H_2 molecule. The system allows for fundamental quantum experiments not accessible in real molecules with the further prospect of quantum control of the electronic properties. Such devices may thus serve as building blocks for future quantum processors.[3]

Since the discovery of single-dot shell structures,[4] electronic properties and many-body effects of electrons confined in two-dimensional parabolic quantum dots have been studied from many different theoretical perspectives and with a great variety of methodological approaches.[5] The first calculations which uncovered the role of the electron-electron interaction were performed in a single dot as early as 1990 and 1991.[6,7] Coupled quantum dots have recently received increasing attention triggered by the experimental verification of controlled qubit operations induced by electromagnetic switches.[3,8] The parabolic coupled quantum dot systems were introduced by Wensauer *et al.*[9] and used for calculating energy levels with the spin-density-functional theory. Based on exact diagonalization techniques, it was later shown that the two-electron ground state exhibits a phase transition from a singlet to a triplet state at finite magnetic-field strengths[10,11] and for interdot distances up to 10 nm. Recently, the stability diagram of a one- and two-electron double quantum dot was calculated for much larger interdot separations (30 and 60 nm) in a related exponential double-well potential.[12]

In this work, we describe the electronic structure of a laterally coupled two-electron quantum dot molecule for different confinement strengths and for varying interdot separations and external electromagnetic fields. The energy spectra and the associated eigenstates are obtained from exact diagonalization of the Hamiltonian in a Hermite polynomial basis set. Some advantages of these basis states are that they form an orthonormal basis set, all matrix elements can be calculated analytically, and the Hamiltonian matrix becomes relatively sparse. Convergence is ensured by comparison with a cylindrical basis expansion method as well as a Fourier split-step operator method based on imaginary time propagation of the four-dimensional Schrödinger equation.[12] The behavior of the spectra when the system is exposed to electric and magnetic fields is then investigated. In the next section, we outline the theoretical methods. The results and their implication for experiments are discussed in Sec. III followed by concluding remarks in Sec. IV.

II. THEORY

The Hamiltonian describing two electrons parabolically confined in a two-dimensional double quantum dot is written as

$$H = h(\mathbf{r}_1) + h(\mathbf{r}_2) + \frac{e^2}{4\pi\epsilon_r\epsilon_0 r_{12}}, \tag{1}$$

with the single-particle Hamiltonian $h(\mathbf{r}_i)$ given as

$$h(x,y) = -\frac{\hbar^2}{2m^*}\nabla^2 + \frac{1}{2}m^*\omega^2 \min\left[\left(x-\frac{d}{2}\right)^2 + y^2, \left(x+\frac{d}{2}\right)^2 + y^2\right] + \frac{e^2}{8m^*}B^2(x^2+y^2) + \frac{e}{2m^*}BL_z + g^*\frac{e}{2m_e}BS_z + eEx. \tag{2}$$

Here, $\mathbf{r}_i=(x_i,y_i)$, $i=1,2$, are the single-particle coordinates in two dimensions, $r_{12}\equiv|\mathbf{r}_1-\mathbf{r}_2|$, m^* is the effective mass of the electron, ω is the confining trap frequency of the harmonic wells, and d is the interdot separation. Furthermore, E is an electric field applied parallel to the interdot axis and B is a magnetic field applied perpendicular to the dot. In the present work, we apply GaAs material parameters with m^*

$=0.067m_e$, relative permittivity $\epsilon_r=12.4$, and an effective g factor $g^*=-0.44$. The potential in Eq. (2), used also in previous studies,[9–11] has a cusp for $x=0$. We have also tested a more realistic smooth barrier and found that no significant changes occur.

It is worth noting that for $d=0$ and in the absence of external fields, the two-electron Hamiltonian can be written in center-of-mass, $\mathbf{R}=\frac{1}{2}(\mathbf{r}_1+\mathbf{r}_2)$, and relative motion, $\mathbf{r}=(\mathbf{r}_1-\mathbf{r}_2)$, coordinates as[14,15]

$$H=-\frac{\hbar^2}{4m^*}\nabla_{\mathbf{R}}^2+m^*\omega^2\mathbf{R}^2-\frac{\hbar^2}{m^*}\nabla_{\mathbf{r}}^2+\frac{1}{4}m^*\omega^2\mathbf{r}^2+\frac{e^2}{4\pi\epsilon_r\epsilon_0|\mathbf{r}|}$$
$$=\frac{1}{2}\left[-\frac{\hbar^2\nabla_{\mathbf{R}}^2}{2m^*}+\frac{1}{2}m^*(2\omega)^2\mathbf{R}^2\right]$$
$$+2\left[-\frac{\hbar^2\nabla_{\mathbf{r}}^2}{2m^*}+\frac{1}{2}m^*\left(\frac{1}{2}\omega\right)^2\mathbf{r}^2\right]+\frac{e^2}{4\pi\epsilon_r\epsilon_0|\mathbf{r}|}. \quad (3)$$

The total wave function then becomes separable as $\Psi(\mathbf{r},\mathbf{R})=\Psi_R^{N,M}(\mathbf{R})\Psi_r^{n,m}(\mathbf{r})$, where $\Psi_R^{N,M}(\mathbf{R})$ is an eigenfunction to the center-of-mass part of Eq. (3) and $\Psi_r^{n,m}(\mathbf{r})$ is an eigenfunction to the relative motion part of Eq. (3), and each is further separable in a radial and an angular part with quantum numbers $n(N)$ and $m(M)$ referring to the radial and angular degrees of freedom, respectively. A state is thus characterized by the four quantum numbers (N,M,n,m) with $(n,N=0,1,\ldots)$ and $(m,M=0,\pm1,\ldots)$, and the total energy can be written as

$$E(N,M,n,m)=(2N+|M|+1)\hbar\omega+(2n+|m|+1)\hbar\omega+E_r(n,m), \quad (4)$$

where the first term originates from the center-of-mass part of Eq. (3), the second term originates from the harmonic oscillator part of the relative motion in Eq. (3), and $E_r(n,m)$ accounts for the electron-electron interaction contribution to the energy. The spatial symmetry of the total wave function under exchange of particle 1 and particle 2 is given by the parity of $\Psi_r^{n,m}(\mathbf{r})$, and thus the spin singlets (triplets) will have even (odd) m. For a more complete description, see, e.g., Taut[14] and Zhu *et al.*[15] In the following, the different calculational schemes used here are outlined.

A. Calculation in Cartesian coordinates

The fact that a large part of the one-electron Hamiltonian [Eq. (2)], without external fields, is diagonal in a harmonic oscillator basis set,

$$h(x,y)\phi_i(x,y)=\hbar\omega\left[n_x+n_y+1+\frac{m^*\omega}{2\hbar}\left(\frac{d}{2}\right)^2\right]\phi_i(x,y)\pm\frac{m^*\omega^2}{2}xd\phi_i(x,y), \quad (5)$$

suggests that a basis representation consisting of products of such one-electron states will be a convenient basis in the diagonalization procedure. We therefore expand the spatial wave function in symmetrized states, which can be associated with the spin singlet and triplet states as

$$|\Psi(\mathbf{r}_1,\mathbf{r}_2)\rangle=\sum_{j\geq i}^{n_{max}}c_{ij}|ij\rangle\otimes|S\rangle, \quad (6)$$

where

$$\langle\mathbf{r}_1,\mathbf{r}_2|ij\rangle=\begin{cases}\frac{1}{\sqrt{2}}[\phi_i(\mathbf{r}_1)\phi_j(\mathbf{r}_2)+(-1)^S\phi_j(\mathbf{r}_1)\phi_i(\mathbf{r}_2)], & i\neq j\\ \phi_i(\mathbf{r}_1)\phi_j(\mathbf{r}_2), & i=j,\end{cases}$$

the c_{ij}'s are the expansion coefficients, and $|S\rangle$ denotes the spin singlet or triplet state, i.e., $|0\rangle$, $|1\rangle$. Operating with Eq. (1) on Eq. (6) and projecting onto a specific total spin lead to the matrix equation $\mathbf{Mc}=E\mathbf{c}$. The coupling matrix elements related to the basis [Eq. (6)] with the Hamiltonian [Eq. (2)] then become a sum of analytical one-electron matrix elements defined by Eq. (5) and matrix elements involving the two-electron interaction,

$$M_{K,L}=\langle\phi_{K_i}\phi_{K_j}|\frac{1}{r_{12}}|\phi_{L_i}\phi_{L_j}\rangle. \quad (7)$$

To solve this integral for arbitrary quantum numbers, we first express the electron-electron interaction as the Bethe integral,[17]

$$\frac{1}{r_{12}}=\frac{1}{2\pi^2}\int\frac{d^3s}{s^2}e^{i\mathbf{s}\cdot\mathbf{r}_1}e^{-i\mathbf{s}\cdot\mathbf{r}_2}. \quad (8)$$

We carry out the integration in the s_z direction and thereafter put $z_1=z_2=0$,

$$\frac{1}{r_{12}}=\frac{1}{2\pi^2}\int d^2s e^{i\mathbf{s}\cdot(\mathbf{r}_1-\mathbf{r}_2)}\int_{-\infty}^{\infty}ds_z\frac{e^{is_z(z_1-z_2)}}{s^2+s_z^2}$$
$$=\frac{1}{2\pi}\int\frac{d^2s}{s}e^{i\mathbf{s}\cdot\mathbf{r}_1}e^{-i\mathbf{s}\cdot\mathbf{r}_2}, \quad (9)$$

where the scalar products (including s^2) now refer to the two-dimensional space. The integral of Eq. (7) can thus be expressed as

$$M_{K,L}=\frac{1}{2\pi}\int\frac{d^2s}{s}\int d^2r_1\phi_{K_i}(\mathbf{r}_1)\phi_{L_i}(\mathbf{r}_1)e^{i\mathbf{s}\cdot\mathbf{r}_1}\times\int d^2r_2\phi_{K_j}(\mathbf{r}_2)\phi_{L_j}(\mathbf{r}_2)e^{-i\mathbf{s}\cdot\mathbf{r}_2}. \quad (10)$$

Introduction of the scaled Hermite polynomials $H_n(x)=2^{n/2}He_n(\sqrt{2}x)$ and the scaling $\tilde{s}=s(2\omega)^{-1/2}$ gives each of the four Fourier transforms the generic form[18]

$$\int_0^{\infty}dvHe_n(v)He_{n+2m}(v)e^{-v^2/2}\cos(\tilde{s}v)=\sqrt{\frac{\pi}{2}}n!(-1)^m\tilde{s}^{2m}e^{-\tilde{s}^2/2}L_n^{2m}(\tilde{s}^2),$$

$$\int_0^\infty dv He_n(v) He_{n+2m+1}(v) e^{-v^2/2} \sin(\tilde{s}v) = \sqrt{\frac{\pi}{2}} n!(-1)^m \tilde{s}^{2m} e^{-\tilde{s}^2/2} L_n^{2m+1}(\tilde{s}^2), \quad (11)$$

with L_a^b a Laguerre polynomial and $v=(2\omega)^{1/2}x$. Here, x denotes any of the variables x_1, y_1, x_2, and y_2 and $\tilde{s}$ denotes $\tilde{s}_x, \tilde{s}_y$. When the operations described by Eqs. (7)–(11) are carried out for four arbitrary one-electron basis states, the result is a combination of four Laguerre polynomials,

$$M_{K,L} = \frac{1}{2\pi} \int \frac{d^2s}{s} \int \frac{d^2\tilde{s}}{\tilde{s}} \tilde{s}_x^{2(K_i+L_i)} \tilde{s}_y^{2(K_j+L_j)} \times L_{a_1}^{b_1}(\tilde{s}_x^2) L_{a_2}^{b_2}(\tilde{s}_y^2) L_{a_3}^{b_3}(\tilde{s}_x^2) L_{a_4}^{b_4}(\tilde{s}_y^2) e^{-v^2}. \quad (12)$$

In total, this shows that the integral is a sum of terms of the form

$$M_{K,L} \propto \int \frac{d^2\tilde{s}}{\tilde{s}} \tilde{s}_x^n \tilde{s}_y^m e^{-\tilde{s}^2} = \int_0^\infty d\tilde{s} \tilde{s}^{n+m} e^{-\tilde{s}^2} \int_0^{2\pi} d\phi \cos^m \phi \sin^n \phi, \quad (13)$$

which are well-known integrals.

By collecting all ω-dependent terms of the potential and the basis functions, one can easily show that the integral scales with the confinement strength as $\omega^{1/2}$. The one-electron integral, cf. Eq. (5), has one term linear in ω (the first diagonal term), one quadratic in ω (the second diagonal term), and one term that depends on $\omega^{3/2}$ (the nondiagonal term). All matrix elements are thus calculated only once for $\omega=1$ and rescaled for every step in the diagonalization process.

In order to compute the field-dependent matrix elements, we need to recall some of the basic properties of Hermite polynomials. To compute the matrix elements for the case with the electric field along the x axis, we need to evaluate single-particle contributions of the form $\langle n_x m_y | Ex | n_x' m_y' \rangle$. Remembering that our single-particle basis functions are (setting $\hbar=1$, $m^*=1$) given by $\phi(x,y) = \frac{\sqrt{\omega}}{\pi^{1/2}\sqrt{n!m!2^n 2^m}} H_n(\sqrt{\omega}x) e^{-\omega/2(x^2+y^2)} H_m(\sqrt{\omega}y)$, we readily obtain

$$\langle nm|Ex|n'm'\rangle = \sqrt{\frac{n'+1}{2\omega}} E \delta_{m,m'} \delta_{n,n'+1} + \sqrt{\frac{n'}{2\omega}} E \delta_{m,m'} \delta_{n,n'-1}. \quad (14)$$

These contributions from each of the two electrons are subsequently added together. For magnetic fields, we take into account both the narrowing of the confining potential arising from the diamagnetic term $\propto \frac{1}{8}B^2r^2$ and the Zeeman term $\propto BL_z$. The matrix elements for the Zeeman term are computed similarly to those for the electric field,

$$\langle nm|L_z|n'm'\rangle = -i\sqrt{n(m+1)}\frac{B}{2}\delta_{m,m'-1}\delta_{n,n'+1} + i\sqrt{m(n+1)}\frac{B}{2}\delta_{m,m'+1}\delta_{n,n'-1}. \quad (15)$$

To account for the diamagnetic term, we notice that the confinement strength of the harmonic oscillator changes from ω to $\omega_{eff}=\sqrt{\omega^2+\omega_C^2}$, where ω_C is the cyclotron frequency $\frac{eB}{2m^*}$. By making the substitution $\omega \to \omega_{eff}$ in the basis functions, we obtain the correct energy for the case with $B \neq 0$. Thus, the diagonal term scales as ω_{eff}, the electron-electron interaction term scales as $\sqrt{\omega_{eff}}$, and the d-dependent term scales as $\omega^2/\sqrt{\omega_{eff}}$. For GaAs parameters, the gyromagnetic ratio is rather small and thus only the $S_z=0$ terms are shown in the results for clarity.

B. Calculation in cylindrical coordinates

To validate the calculations, we have also treated the single quantum dot with an alternative method where the radial wave functions are expressed in the so-called B splines. The solutions to the single-particle Hamiltonian [Eq. (2)] with $d=0$ and $E=0$ can be written as

$$|\Psi_{nmm_s}\rangle = |u_{nmm_s}(r)\rangle |e^{im\phi}\rangle |m_s\rangle, \quad (16)$$

where the radial parts of the wave functions are expanded in B-splines,[19]

$$|u_{nmm_s}(r)\rangle = \sum_{i=1} c_i |B_i(r)\rangle, \quad (17)$$

on a so-called knot sequence and they form a complete set in the space defined by the knot sequence and the polynomial order.[19] Here, we have typically used 40 points in the knot sequence, distributed linearly in the inner region and then exponentially further out. The last knot, defining the box size to which we limit our problem, is placed at a distance of about 400 nm from the center. The polynomial order is 6 and combined with the knot sequence this yields 33 radial basis functions $u_{nmm_s}(r)$ for each combination (m,m_s). The basis functions associated with lower energies are physical states, here thus two-dimensional harmonic oscillator eigenstates, while those associated with higher energies are determined mainly by the box. The unphysical high-energy states are, however, still essential for the completeness of the basis set. Equations (16) and (17) imply that the Schrödinger equation can be written as a matrix equation $\mathbf{Hc}=\epsilon\mathbf{Bc}$, where $H_{ij}=\langle B_i e^{im\theta}|h|B_j e^{im\theta}\rangle$ and $B_{ij}=\langle B_i|B_j\rangle$. This equation is a generalized eigenvalue problem that can be solved with standard numerical routines. The integrals are calculated with Gaussian quadrature yielding essentially no numerical error since B-splines are piecewise polynomials.

The eigenstates of the matrix equation form a complete orthogonal basis set for each pair of quantum numbers m, m_s which can be used to diagonalize the two-particle Hamiltonian [Eq. (1)]. We then get matrix elements of the form

$$H_{ij} = \langle \{ab\}_i | h(1) + h(2) + \frac{1}{r_{12}} | \{cd\}_j \rangle, \tag{18}$$

where the last term refers to the last term in Eq. (1). Each single-particle state is of the form of Eq. (16), and we use the multipole expansion suggested by Cohl *et al.*[20] to get an explicit expression for the last term,

$$\langle ab | \frac{1}{r_{12}} | cd \rangle = \frac{e^2}{4\pi\epsilon_r\epsilon_0} \langle u_a(r_i) u_b(r_j) | \frac{Q_{m-1/2}(\chi)}{\pi\sqrt{r_i r_j}} | u_c(r_i) u_d(r_j) \rangle \times \langle e^{im_a\phi_i} e^{im_b\phi_j} | \sum_{m=-\infty}^{\infty} e^{im(\phi_i - \phi_j)} | e^{im_c\phi_i} e^{im_d\phi_j} \rangle \times \langle m_s^a | m_s^c \rangle \langle m_s^b | m_s^d \rangle. \tag{19}$$

Here, $Q_{m-1/2}(\chi)$, with $\chi = \frac{r_1^2 + r_2^2 + (z_1 - z_2)^2}{2 r_1 r_2}$, are Legendre functions of the second kind and half-integer degree. We evaluate them using a modified[21] version of software DTORH1.F described by Segura and Gil.[22] The matrix is diagonalized for a given value of $M_L = m(1) + m(2)$, including up to $|m| \leqslant 6$, and $M_S = m_s(1) + m_s(2)$. For zero magnetic field, the $S = 0, 1$ states are characterized by symmetric and antisymmetric spatial wave functions, respectively. The dimension of the matrix to diagonalize is, with the choice of 40 points in the knot sequence, up to $\sim 14\,000 \times 14\,000$. To compare with the solutions in Cartesian coordinates, we limit the number of basis states in the same way as in the Cartesian case, but we have also compared these results to what is obtained when the complete B-spline basis set is used.

C. Imaginary time propagation

To provide yet another reference value for the singlet ground-state energy, we have also performed a calculation based on imaginary time propagation.[13] Consider the formal solution to the time-dependent Schrödinger equation for a time-independent system expanded in the eigenstates,

$$|\Psi(t)\rangle = e^{-iHt/\hbar} |\Psi(0)\rangle = \sum_j c_j e^{-iE_j t/\hbar} |\phi_j\rangle. \tag{20}$$

When the substitution $\tau = -it$ is performed and $|\Psi(\tau)\rangle$ is propagated in a standard time propagator, all states with higher energy than the ground state will be damped exponentially compared to the ground state. Therefore, $|\Psi(\tau)\rangle / \sqrt{\langle \Psi(\tau) | \Psi(\tau) \rangle}$ will converge toward the ground state. Furthermore, when the solution has converged, the ground-state energy is obtained from

$$E_0 = -\frac{1}{2\Delta\tau} \log\left(\frac{\langle \Psi(\tau + \Delta\tau) | \Psi(\tau + \Delta\tau) \rangle}{\langle \Psi(\tau) | \Psi(\tau) \rangle} \right), \tag{21}$$

where $\Delta\tau$ is the time step used in the propagation. In the calculations, a four-dimensional Cartesian Fourier split-step propagator is used, with which convergence was found employing a grid of size $(100 \times 50) \times (100 \times 50)$, 8 nm grid spacing, and propagation time step $\Delta\tau = 44$ fs. By applying this method, we obtain the singlet ground-state energy as a function of dot separation d.

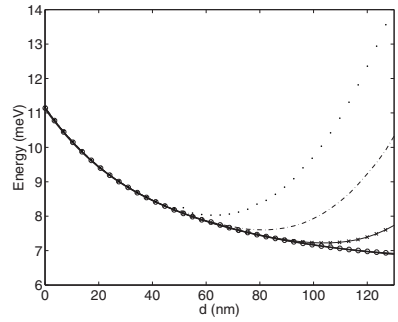

FIG. 1. Ground-state energy for different Cartesian basis sizes as function of interdot distance compared with the results from imaginary time propagation. Dotted line: $n_{max} = 5$. Dashed-dotted line: $n_{max} = 7$. Full line with crosses: $n_{max} = 10$. Circles: $n_{max} = 15$. Solid black line: Imaginary time propagation. The confinement strength $\hbar\omega = 3$ meV.

D. Validation of method

A weakness of all single-center expansions is the large number of basis states required to describe the spectrum accurately for large interdot distances. As a convergence check, we show in Fig. 1 a comparison between the distance-independent imaginary time method and various basis sizes of the Cartesian basis for a double well with confining strength $\hbar\omega = 3$ meV. Increasing d is seen to require increasing n_{max} to obtain convergence of the ground state: While for $n_{max} = 5$ the calculation breaks down already at 60 nm, $n_{max} = 10$ is seen to work satisfactory up to 100 nm. In the following, the calculations are thus based on $n_{max} = 10$ with some selected control calculations with $n_{max} = 15$. The latter amount to a $50\,625 \times 50\,625$ matrix, which is diagonalized with an ARPACK sparse matrix solver.[23] With the $n_{max} = 15$ basis, the truncation error is kept small for interdot distances up to about 140 nm when considering the lower part of the energy spectrum ($\hbar\omega = 3$ meV).

For the case of noninteracting particles, we have tested the effect of having a smooth potential barrier between the coupled dots, see Fig. 2. The inset gives a close-up view of the barrier for $d = 52$ nm, either in form of a cusp or in a smoother version. The ground-state energies for both cases are also shown, and they can hardly be distinguished. Figure 2 also shows the ground state as a function of d. As expected, the difference in ground-state energy is largest when the energy level is close to the barrier height (around $d = 50$ nm), but still it is everywhere on the subpercentage level. We conclude that the qualitative properties of the coupled dots will not be affected by the cusp and a better modeling is only justified when experimental information on the barrier is available.

The spectra of the cylindrical and Cartesian basis calculations have also been compared, and the results for $d = 0$ are shown in Tables I and II for $B = 0$ and $B = 3$ T, respectively. For $d = 0$, we note that in both cases, the energy spacing

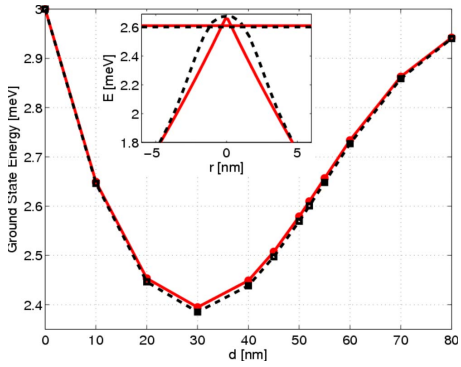

FIG. 2. (Color online) The ground-state energy for a single electron in a double dot ($\hbar\omega$=3 meV) as a function of interdot distance d. The solid (red) line shows the result with a sharp boundary between the two dots, while the dashed (black) line shows the result when the boundary is smoothed. The difference in ground-state energy is largest when the ground-state energy is close to the barrier height, around d=50 nm, but still it is everywhere on the subpercentage level. The inset shows the sharp (solid red line) and the smoothed (dashed black line) barrier for d=52 nm with the corresponding ground-state energies indicated by the horizontal lines.

between the two lowest states equals $\hbar\omega$ for the singlet as well as for the triplet series. The first-order energy contribution is identical for the two lowest singlets and the two lowest triplet states, which implies that the energy spacing between the lowest levels to first order is exactly $\hbar\omega$. This is the expected spacing for confinement strengths $\hbar\omega$ larger than 1 meV when the energy level ordering is largely determined by the harmonic potential. For weaker confinement strengths, the electron-electron interaction will play a larger role, and the $\hbar\omega$ splitting will no longer be observed.[15]

TABLE I. Ten lowest-energy levels (given in meV), azimuthal quantum number, and total spin for the confinement strength $\hbar\omega$ =3 meV, d=0, and B=0.

Energy (meV)		State	
Cartesian basis	Cylindrical basis	M_L	S
11.155	11.147	0	0
12.408	12.407	1	1
12.408	12.407	−1	1
14.158	14.149	1	0
14.158	14.149	−1	0
14.682	14.681	2	0
14.682	14.681	−2	0
15.409	15.407	−2	1
15.409	15.407	2	1
15.408	15.407	0	1

TABLE II. Twelve lowest-energy levels (given in meV), azimuthal quantum number, and total spin for the confinement strength $\hbar\omega$=3 meV, d=0, and B=3 T. At this field strength, the total spin is still an approximately good quantum number and each state can be assigned a specific total spin.

Energy (meV)		State	
Cartesian basis	Cylindrical basis	M_L	S
13.262	13.261	−1	1
13.774	13.740	−2	0
14.063	14.052	0	0
14.635	14.634	−2	1
14.670	14.670	−3	1
15.147	15.146	−3	0
15.440	15.427	−1	0
15.732	15.732	−4	0
16.009	16.007	−3	1
16.043	16.042	−4	1
16.520	16.519	−4	0
16.817	16.803	−2	0

The tabulated Cartesian coordinate values are calculated with n_{max}=10. With the cylindrical coordinate method, both $|m|_{max}$ and the number of radial basis functions (n_r) are adjusted to include the same physical states as used with the Cartesian coordinate method. For this, we use the relations $n_r=n_x+n_y-\max(n_x,n_y)$ and $m=n_x-n_y$. The energies are in very satisfactory agreement, with a relative difference of less than 1% for all considered levels. With the B-spline basis, it is also possible to saturate the radial basis set and compare the results to the truncated ones. We then use $|m|\leqslant 6$ and the full set of 33 radial basis functions (for a knot sequence of 40 points). The ground state then changes from 11.147 to 11.140 meV, and the last tabulated state changes from 15.4069 to 15.4065 meV, which shows that the basis-set expansion is indeed converged to within less than 1%.

III. RESULTS

A. Field-free case

Figure 3 shows the 12 lowest-energy levels as a function of interdot distance in the case of two noninteracting particles (with $\hbar\omega$=3 meV) and in the case of interacting electrons with three different confinement strengths, $\hbar\omega$=1, 3, and 6 meV. The spectra with and without electron interaction are seen to differ strongly: In the case of $\hbar\omega$=3 meV, the ground-state energy increases from 6 to 11.15 meV for d=0 and to 7.5 meV for d=80 nm. Comparing the spectra for the three confinement strengths, we discover some common features. At d=0, the first excited energy level consists, for the case of noninteracting particles, of four degenerate states, i.e., two singlet and two triplet states. However, when the particle interaction is taken into account, the singlet and triplet levels split in energy in the same manner as the energy

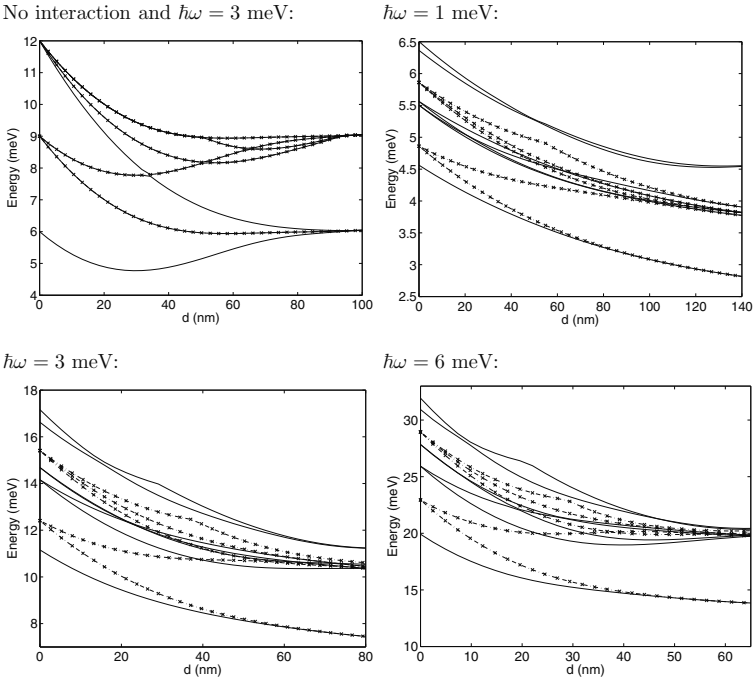

FIG. 3. Energy spectrum as a function of d for the two lowest bands of states and for varying confinement strengths $\hbar\omega$. Full lines: Singlet states. Broken lines with crosses: Triplet states.

levels of atomic helium split into parahelium (singlet) and orthohelium (triplet) levels, with the triplet state always lying lower in energy than the corresponding singlet state. The first excited state becomes a degenerate triplet state, corresponding to cylindrical basis states with conserved quantum numbers $M = \pm 1$. For a more detailed discussion of the spectrum of the two- and three-dimensional harmonic oscillator containing two electrons, we refer to Zhu *et al.*[15] and Drouvelis *et al.*[16]

At finite $d > 0$, the rotational symmetry is broken and, correspondingly, the first excited doubly degenerate triplet level split, with one level gradually decreasing in energy toward the singlet ground-state energy and becoming virtually degenerate with it at large inter-dot distances. This gives rise to a ground-state energy band. In Table III, we list the 32 lowermost states in groups for $d = 80$ nm. Above the nearly degenerate ground-state level, there is a group of eight excited states that are seen to constitute a narrow band of singlet and triplet states for large interdot distances. The energy spacing between the ground-state band and the second band is seen to be of the order $\hbar\omega$.

In Fig. 4, the configuration interaction (CI) one-electron probability density $\rho(\mathbf{r}_1) = \int d^2 r_2 |\Psi(\mathbf{r}_1, \mathbf{r}_2)|^2$ is shown for the ten lowest states at $d = 80$ nm and $\hbar\omega = 3$ meV. These are obtained from a straightforward analytical integration (to unity or zero) of the basis multiplied with the relevant weight of each eigenvector component. The ground states are dominantly described by combinations of two ground states of each harmonic oscillator, representing one electron in each well. The states of the excited band is seen to consist of combinations of dipolar two-center states oriented parallel or

TABLE III. Energy levels (given in meV) and spin (in parentheses) of the 32 lowest states for $d = 80$ nm and $\hbar\omega = 3$ meV, grouped into five bands.

Band number	Energy (spin)			
1		7.3127(0)	7.3124(1)	
2	10.253(0)	10.253(1)	10.313(0)	10.313(1)
	10.376(0)	10.404(1)	10.507(0)	10.530(1)
3		11.240(0)	11.245(0)	
4	12.413(1)	12.416(1)	12.417(1)	12.450(1)
5	13.205(0)	13.205(1)	13.253(0)	13.253(1)
	13.313(0)	13.313(1)	13.331(0)	13.354(1)
	13.377(0)	13.403(1)	13.425(0)	13.442(1)
	13.508(0)	13.530(1)	13.515(0)	13.672(1)

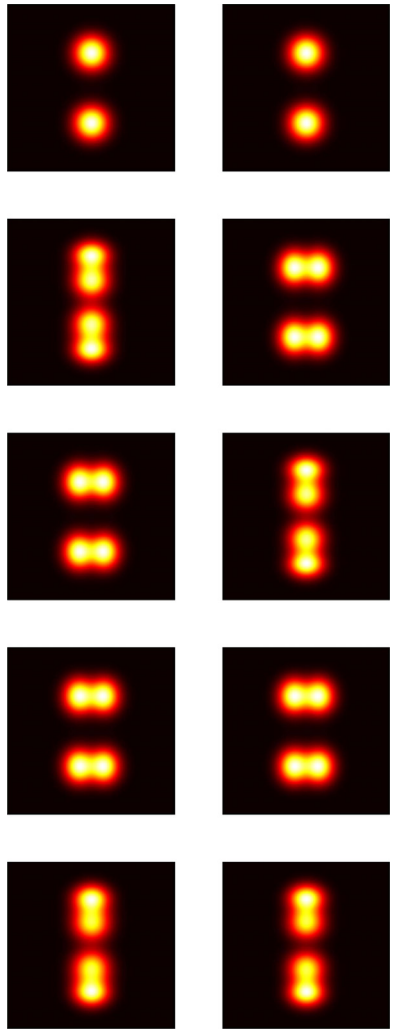

FIG. 4. (Color online) CI single-particle electron probability density distributions for the two lowest-energy bands at $d=80$ nm. Singlet states are in the left column, triplets in the right. The states are ordered with energies increasing from top to bottom.

perpendicular to the interdot direction. Very little differences in shape of the singlets vs triplets are observed. The energy ordering is, however, different between the singlets and the triplets.

The upbuilding of the two lowest bands at large d's are readily understood in terms of a Heitler-London ansatz: The two states in the first band are constructed from the spatially symmetric and antisymmetric combinations of single-electron ground states in each well,

$$\Psi_{\pm}(\mathbf{r}_1,\mathbf{r}_2) \propto \phi_{00}(\mathbf{r}_{1L})\phi_{00}(\mathbf{r}_{2R}) \pm \phi_{00}(\mathbf{r}_{2L})\phi_{00}(\mathbf{r}_{1R}), \quad (22)$$

forming the so-called covalent states. The subscripts on the vectors refer to particle number and well, i.e., $\mathbf{r}_{iL}=\mathbf{r}_i+\frac{1}{2}\mathbf{d}$ and $\mathbf{r}_{iR}=\mathbf{r}_i-\frac{1}{2}\mathbf{d}$, $i=1,2$. The energy of these two states is asymptotically given as $E_0=2\hbar\omega+\frac{e^2}{4\pi\epsilon_r\epsilon_0}\frac{1}{d}$, since the exchange energy will vanish, and the wave function in each well becomes pointlike when observed from the other well. Within this model, the contribution from the Coulomb energy amounts to about 1.5 meV at 80 nm and the total energy would then be 7.5 meV for a $\hbar\omega=3$ meV double dot. Thus, this simple model generates an energy within 3% of the CI energy of 7.3 meV (see Table III). Such a model of the two lowest-energy states was also considered by Wensauer *et al.*,[9] where the energy expectation value was calculated using perturbation theory.

Continuing the procedure of Eq. (22), we now build up the states in the second band from excited two-center harmonic oscillator states, with one electron located in each dot,

$$\phi_{ij}(\mathbf{r}_{1L})\phi_{kl}(\mathbf{r}_{2R}), \quad (23)$$

where one of i, j, k, and l is equal to 1 and the others zero. These product states are combined to yield correctly symmetrized wave functions, with even or odd parity. This gives rise to totally eight different states, of which four are singlets and four are triplets. For example, the first excited singlet state in the energy spectrum, which has odd parity, would be

$$\Psi(\mathbf{r}_1,\mathbf{r}_2) \propto \phi_{10}(\mathbf{r}_{1L})\phi_{00}(\mathbf{r}_{2R}) + \phi_{00}(\mathbf{r}_{1L})\phi_{10}(\mathbf{r}_{2R}) + \phi_{10}(\mathbf{r}_{1R})\phi_{00}(\mathbf{r}_{2L}) + \phi_{00}(\mathbf{r}_{1R})\phi_{10}(\mathbf{r}_{2L}), \quad (24)$$

with the energy asymptotically given by $E=3\hbar\omega+\frac{e^2}{4\pi\epsilon_r\epsilon_0}\frac{1}{d}$.

In Fig. 5, the CI one-electron probability density is exposed in more detail for the first excited singlet state (left column, second row) of Fig. 4. Also shown is the corresponding one-electron density corresponding to the ansatz state of Eq. (24), as well as one-dimensional slices or conditional densities[11] of the respective wave functions. These are produced by finding the maxima of the wave function and evaluating it there for all but one degree of freedom. The two curves in panels 3 and 4 depict one out of the four maxima in the wave function, evaluated for both electrons. The overall agreement between the model and the CI densities is in general, very good. This is also the case for any of the other states of the first excited band. We clearly see that the two electrons indeed occupy separate wells. In addition, we observe in the CI figure a small probability for the electrons to be situated in the same well, a feature not present in the model figure.

In contrast to the two lowest bands, the third band containing two singlet states has a high probability of having both electrons in the same well, forming the so-called ionic states. The energy of these states will, with increasing interdot distance, converge toward the single-dot two-electron

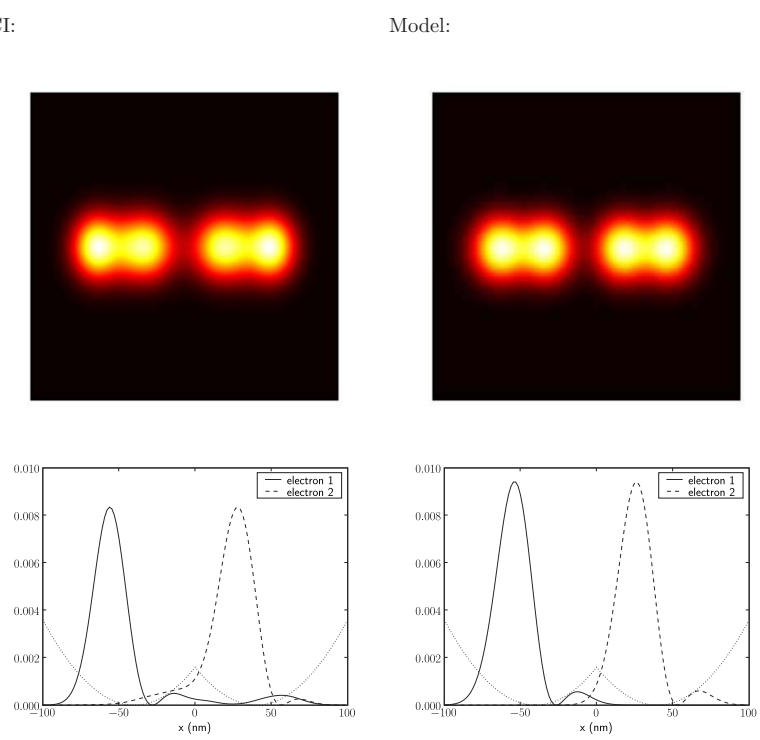

FIG. 5. (Color online) The CI one-electron probability density exposed in more detail for the state on the left column, second row of Fig. 4. Also shown is the corresponding one-electron density of the Heitler-London model. The lower panels show the conditional densities of each electron and their positioning relative to the potential (dotted line).

ground state. When considering higher bands, we see that the situation becomes more complex which is due to the fact that the states approach the cusp energy and are thus a complex mixture of states with two electrons in a single well and one electron in each well. At even higher energies far above the cusp, the spectrum will gradually approach the level structure of a single harmonic oscillator.[16]

The present results can be compared to previous studies with spin-density-functional theory (SDFT).[9] For larger dot separations, the results obtained there differ from those presented here; the band structure found here cannot be inferred from the results in Ref. 9, and, in addition, the SDFT calculation yields a triplet ground state for dot separations larger than ~45 nm while the present ground state is of the expected singlet symmetry for all distances. It is argued in Ref. 9 that the polarized ground state is an artifact of the self-energy within the SDFT scheme, i.e., that it stems from the unphysical interaction of a single electron with its own Coulomb field. According to the results shown in Figs. 3 and 4 of Ref. 9, this affects the long-range energies of a $\hbar\omega=3$ meV double dot at least on the 1 meV level. The approximate exchange and correlation used in DFT calculations is apparently not enough to ensure correct separation energies of the two dots, and the fact that the band structure is not found in Ref. 9 is thus probably due to this deficiency.

An interesting aspect is to what extent the present band structure is general for all two-center potentials, and whether, for example, quadratic or exponential double-well potentials will also reproduce similar upbuilding. This is a relevant issue with respect to the very simple level structure behind the modeling applied by Petta *et al.*[2]

B. Structure with electromagnetic fields

The response of the electronic structure and dynamics to magnetic fields has been studied in a number of recent works.[5,10,11,24] We show in Fig. 6 the lowest part of the energy spectrum as a function of magnetic-field strength for three different values of d. The upper figure for $d=0$ shows virtually identical results with those of Helle *et al.*[11] and also the singlet-triplet ground-state transition at around $B=2$ T, which was pointed out by these authors. In addition, we note

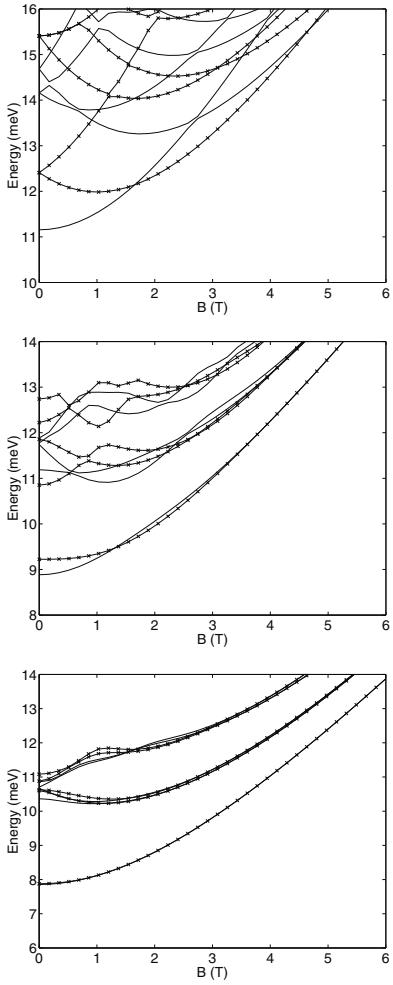

FIG. 6. Energy spectrum as a function of B, for interacting electrons, with $d=0$ nm (upper), $d=30$ nm (middle), and $d=60$ nm (lower). $\hbar\omega=3$ meV in all panels. Full lines: Singlet states. Full lines with crosses: Triplet states.

the strong variation of the energy levels with magnetic-field strength following from the competition between the linear (Zeeman) and quadratic (diamagnetic) terms in Eq. (2): For strong enough field strengths, the diamagnetic term gives rise to a linear increase in the energy as it modifies the effective confinement strength $\omega \rightarrow \sqrt{\omega^2+[eB/(2m^*)]^2}$. At weak fields, the Zeeman term dominates which effectively modifies each state energy by $e\hbar B/2m^*M$. Thus, states with negative (positive) M quantum number decrease (increase) in energy with increasing B field which, in total, leads to a series of (avoided) crossings until the diamagnetic term becomes significant.

In the middle and lower parts of the panel, we plot the energy spectrum for $d=30$ and $d=60$ nm. At these distances, the Zeeman term is less pronounced, since angular momentum is not conserved. Each state consists of several angular momentum components which contribute differently to the energy and tend to wash out a strong dependence. However, the states of the first excited band groups have a positive or negative angular momentum expectation value. Thus, the eight state bands split into two subbands each containing four states. The band structure is, however, not destroyed by the magnetic field, and thus, in some sense, magnetic effects are less pronounced at large interdot distances than at small distances. At higher field strengths, the diamagnetic term is seen to cause an increase in energy for all levels, but level ordering is determined by the Zeeman term.

Several recent experiments[2,8] apply electric fields to guide the electron loading into one of the dots as well as to steer the electron between selected quantum states. In this context, controlled dynamics requires understanding of the nature of the time evolution of the quasiadiabatic states and potential avoided crossings with respect to the switching times,[24] as well as various couplings to the environment, such as spin-spin coupling between the electron spins and the $\sim 10^6$ nuclear spins from the surrounding material, typically GaAs.[2]

In Fig. 7, we display the energy spectrum as a function of electric-field strength for an electric field directed along the interdot axis. For all panels, we observe a nondegenerate singlet state as ground state for large fields since the Pauli principle prevents a two-electron one-center triplet ground state. At $d=0$ (top panel), the electric field is seen to only shift the spectrum up or down, i.e., the energy differences between states are not influenced by the electric field. At larger interdot distances, the situation, in contrast to the magnetic case, becomes more complex. The bottom of both potential wells will now be shifted spatially and changed in energy. One will be lifted and shifted toward the origin, while the other is lowered and shifted away from the origin, depending on the sign of the electric field. When the electric field becomes very strong, there will, in effect, be only one well centered far away from the origin. Consequently, the spectrum approaches that of two interacting electrons in a single harmonic oscillator potential. This can be seen by comparing the lowest panel in Fig. 7 with Fig. 3.

As an example, we plot in Fig. 8 the single-particle electron probability density for the lowest singlet state at $d=60$ nm for selected field strengths. Around $|E| \sim -0.1$ mV/nm (upper panel), the electronic density distribution is seen to be localized in one of the wells. At $E=-0.05$ mV/nm (middle panel), we see a small fraction of the density occupying the second well. Finally (bottom), a fully delocalized two-center state is shown for $E=0$. The transition from a one-well state to a two-center state goes through a single or a series of avoided crossings. In experiments where an initial electric field is applied to load two electrons into a single-well ground state, followed by a fast

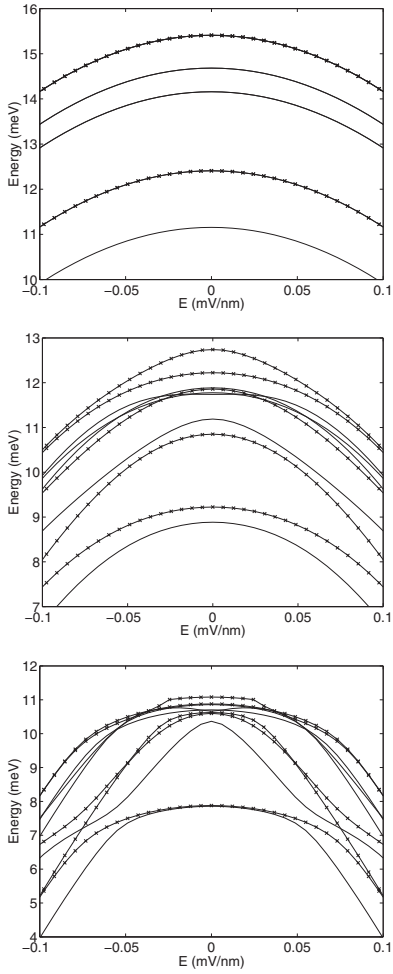

FIG. 7. Energy spectrum as a function of electric-field strength E for the two interacting electrons with $d=0$ nm (top), $d=30$ nm (middle), and $d=60$ nm (bottom). The confinement strength $\hbar\omega=3$ meV in all panels. Full lines: Singlet states. Full lines with crosses: Triplet states.

switch of the field, there may thus be a sizable probability for transfer from the lowest to the first excited singlet state while the system traverses avoided crossings. The part of the system which follows the ground state is shown by Petta *et al.*[2] to mix strongly with the triplet state through spin-spin couplings with the surrounding nuclei. By alternatively applying electromagnetic switches which guide the system via diabatic transitions, the singlet-triplet mixing may be suppressed.

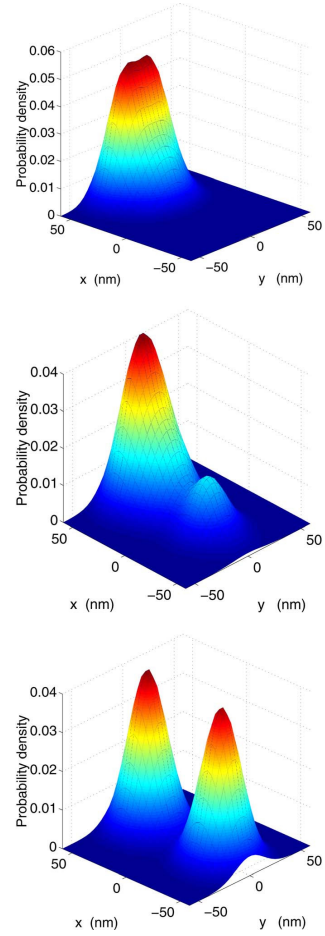

FIG. 8. (Color online) Single-particle electron probability density for three different electric-field strengths $E=-0.08$ mV/nm (top), $E=-0.06$ mV/nm (middle), and $E=0$ (bottom). The confinement strength $\hbar\omega=3$ meV, and $d=60$ nm.

IV. CONCLUDING REMARKS

In the present paper, we have developed a method for diagonalizing the Schrödinger equation of two electrons in a parabolically confined two-center quantum dot. The method is verified by comparison with related basis-set and grid-based calculations. The particular analytical properties of the Cartesian basis method allow for rapid and accurate calculation of energy spectra of the quantum dot two-center system with basis sizes above 50 000states.

Diagonalization of the Hamiltonian for increasing well separation shows that above the degenerate singlet and triplet

ground states, there is a narrow band of four singlet and four triplet states. The energy spacing between the ground state and the first excited band scales directly with the confinement strength of each quantum well. From symmetry considerations, this structure is expected for any two-dimensional two-center potentials which are asymptotically spherical and with similar relative strength of the electron-electron interaction. Calculations of the energy levels for large interdot distances in the presence of magnetic fields show that this band structure dominates for any magnetic-field strength. In contrast, an electric field parallel to the interdot direction results in strong level mixing, and the transition from a localized "ionic" state to a covalent state occurs in a narrow range of electric-field strengths.

ACKNOWLEDGMENTS

The present research has been partially sponsored by the Norwegian Research Council through the NANOMAT program and the Nordic Research Board NordForsk. E.L. and E.W. gratefully acknowledge financial support from the Swedish Research Council (VR) and from the Göran Gustafsson Foundation.

[1] M. Bayer *et al.*, Science **291**, 451 (2001); W. J. M. Naber, T. Fujisawa, H. W. Liu, and W. G. van der Wiel, Phys. Rev. Lett. **96**, 136807 (2006).
[2] J. R. Petta *et al.*, Science **309**, 2180 (2005).
[3] D. Loss and D. P. DiVincenzo, Phys. Rev. A **57**, 120 (1998).
[4] S. Tarucha, D. G. Austing, T. Honda, R. J. van der Hage, and L. P. Kouwenhoven, Phys. Rev. Lett. **77**, 3613 (1996).
[5] S. M. Reimann and M. Manninen, Rev. Mod. Phys. **74**, 1283 (2002).
[6] U. Merkt, J. Huser, and M. Wagner, Phys. Rev. B **43**, 7320 (1991).
[7] A. Kumar, S. E. Laux, and F. Stern, Phys. Rev. B **42**, 5166 (1990).
[8] M. Bayer *et al.*, Science **291**, 451 (2001); F. H. L. Koppens *et al.*, Nature (London) **435**, 766 (2006).
[9] A. Wensauer, O. Steffens, M. Suhrke, and U. Rössler, Phys. Rev. B **62**, 2605 (2000).
[10] A. Harju, S. Siljamäki, and R. M. Nieminen, Phys. Rev. Lett. **88**, 226804 (2002).
[11] M. Helle, A. Harju, and R. M. Nieminen, Phys. Rev. B **72**, 205329 (2005).
[12] L. X. Zhang, D. V. Melnikov, and J. P. Leburton, Phys. Rev. B **74**, 205306 (2006).
[13] A. K. Roy, N. Gupta, and B. M. Deb, Phys. Rev. A **65**, 012109 (2002).
[14] M. Taut, Phys. Rev. A **48**, 3561 (1993).
[15] J. L. Zhu, Z. Q. Li, J. Z. Yu, K. Ohno, and Y. Kawazoe, Phys. Rev. B **55**, 15819 (1997).
[16] P. S. Drouvelis, P. Schmelcher, and F. D. Diakonos, Europhys. Lett. **64**, 232 (2003).
[17] See, e.g., B. H. Bransden and C. J. Joachain, *Physics of Atoms and Molecules* (Prentice-Hall, Malaysia, 2003), p. 709.
[18] A. Erdely *et al.*, *Tables of Integral Transforms* (McGraw-Hill, New York, 1954).
[19] C. deBoor, *A Practical Guide to Splines* (Springer-Verlag, New York, 1978).
[20] H. S. Cohl, A. R. P. Rau, J. E. Tohline, D. A. Browne, J. E. Cazes, and E. I. Barnes, Phys. Rev. A **64**, 052509 (2001).
[21] It is modified in the sense that the limit of how close to 1 the argument χ can be is changed. This is simply so that sufficient numerical precision can be achieved.
[22] J. Segura and A. Gil, Comput. Phys. Commun. **124**, 104 (1999).
[23] http://www.caam.rice.edu/software/ARPACK/
[24] M. Førre, J. P. Hansen, V. Popsueva, and A. Dubois, Phys. Rev. B **74**, 165304 (2006).